Laboratory Kinetic and Mechanistic Studies on the OH-Initiated Oxidation of Acetone in Aqueous Solution

ARTICLE *in* THE JOURNAL OF PHYSICAL CHEMISTRY A · MARCH 2012

Impact Factor: 2.69 · DOI: 10.1021/jp2120753 · Source: PubMed

4 AUTHORS, INCLUDING:

J. Schindelka
Leibniz Institute for Tropospheric Research
12 PUBLICATIONS **45** CITATIONS
SEE PROFILE

Hartmut Herrmann
Leibniz Institute for Tropospheric Research
745 PUBLICATIONS **6,949** CITATIONS
SEE PROFILE

THE JOURNAL OF PHYSICAL CHEMISTRY A

Article

pubs.acs.org/JPCA

Laboratory Kinetic and Mechanistic Studies on the OH-Initiated Oxidation of Acetone in Aqueous Solution

Thomas Schaefer, Janine Schindelka, Dirk Hoffmann,‡ and Hartmut Herrmann*

Leibniz-Institut für Troposphärenforschung (IfT), Abteilung Chemie, Permoserstrasse 15, D-04318 Leipzig, Germany

ABSTRACT: The OH-initiated oxidation of acetone in aqueous solution is investigated because of its potential implications in atmospheric chemistry. The UV-spectrum of the transient acetonylperoxy radical was measured. Two characteristic absorption bands of the acetonylperoxy radical spectrum are found in the 220−400 nm wavelength region. The rate constant for the recombination reaction of the acetonylperoxy radical was determined as a function of temperature for the first time in aqueous solution with $k_{rec,298\ K} = (7.3 \pm 1.3) \times 10^8\ M^{-1}\ s^{-1}$, $E_A = 4.5 \pm 3.3$ kJ mol^{-1}, and $A = (4.7 \pm 2.7) \times 10^9\ M^{-1}\ s^{-1}$. Furthermore, kinetic investigations of the OH-initiated oxidation of methylglyoxal and pyruvic acid were performed with the following results: for methylglyoxal, $k_{second} = (6.2 \pm 0.2) \times 10^8\ M^{-1}\ s^{-1}$, $E_A = 12 \pm 2$ kJ mol^{-1}, and $A = (7.8 \pm 0.2) \times 10^9\ M^{-1}\ s^{-1}$; for pyruvic acid (pH = 0), $k_{second} = (3.2 \pm 0.6) \times 10^8\ M^{-1}\ s^{-1}$, $E_A = 15 \pm 5$ kJ mol^{-1}, and $A = (1.1 \pm 0.1) \times 10^{11}\ M^{-1}\ s^{-1}$; for pyruvate (pH = 6), $k_{second} = (7.1 \pm 2.4) \times 10^8\ M^{-1}\ s^{-1}$, $E_A = 25 \pm 19$ kJ mol^{-1}, and $A = (1.5 \pm 0.4) \times 10^{13}\ M^{-1}\ s^{-1}$. Quantitative product studies were done as a function of the number of laser photolysis pulses for acetone and its oxidation products methylglyoxal, hydroxyacetone, pyruvic acid, acetic acid, and oxalic acid. After the recombination reaction of acetonylperoxy radicals, there are two possible decomposition reactions where the primary products methylglyoxal and hydroxyacetone are formed. From product analysis after a single photolysis laser shot, the ratio of the main product-forming reactions was determined as (A) 30% and (B) 56% for the methylglyoxal formation via channel A to yield two molecules of methylglyoxal and channel B to yield one molecule of methylglyoxal and one molecule of hydroxyacetone. The remaining product can be ascribed to channel C, the radical-retaining channel forming alkoxy radicals with a yield of 14%. Pyruvic acid and acetic acid were found to be the major intermediates estimated with concentrations in the same order of magnitude and a similar time profile, indicating that acetic acid is also a possible oxidation product of methylglyoxal.

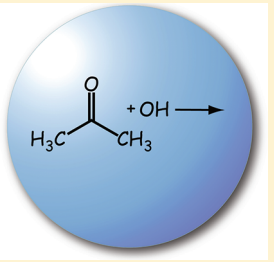

INTRODUCTION

Since the troposphere is a complex mixture of gas phase molecules and dispersed liquid and solid particles, not only the chemical conversion in the gas phase need to be understood, but those in the full multiphase system as well. Volatile organic compounds (VOCs) are important trace gases emitted by biogenic as well as anthropogenic sources. The chemistry of VOCs is of interest as they can produce HO_x and ozone during their oxidation processes and therefore have an impact on the oxidizing capacity of the atmosphere. In addition, VOC oxidation products can contribute to the formation of secondary organic aerosol (SOA) by participating in gas-to-particle partitioning processes.

Atmospheric organic aerosols play a substantial role in atmospheric processes. They can have a direct or indirect effect on the radiation budget and climate, as they can absorb or scatter light and serve as condensation nuclei for cloud formation. Tropospheric multiphase reactions can also have a significant impact on the concentration and distribution of trace gases.[1,2]

With mean concentrations of 0.2−3 ppbv, acetone is a commonly occurring oxygenated compound in the troposphere.[3−6] It is mainly emitted directly from the biosphere, but the oxidation of isoalkanes released from anthropogenic sources also contributes to the high source flux of 95 Tg C a^{-1}.[3,6] The main sinks of acetone are the reaction with OH radicals and the photolysis.[7] In the lower troposphere, the reaction with OH radicals is a significant but slow removal process leading to the formation of smaller, functionalized organic compounds. As has been shown before, the photolysis of acetone after its escape from the boundary layer has strong impacts on atmospheric chemistry. Acetone photolysis controls its lifetime in the free and upper troposphere, which can vary between a few days and one month depending on the season, the latitude and altitude.[8] The photolysis of acetone is an important source for the production of HO_x and a key precursor compound for peroxyacetyl nitrate (PAN), and thus has a strong effect on the oxidizing capacity of the troposphere.[4,9−11]

Different from the gas phase, there are only a few studies on the significance of aqueous phase oxidation processes for the degradation of acetone in the troposphere. Analogous to the gas phase, the main sink in the aqueous phase is the OH-initiated oxidation. The majority of studies deal with the characterization of the kinetics of the hydroxyl radical reactions[12−15] and only a small number of studies are concerned with the analysis of the resulting products.[16−19] One reason is the Henry coefficient of acetone ($H_{Acetone} = 32$ M atm^{-1}), which could be regarded as small, thus suggesting that

Special Issue: A. R. Ravishankara Festschrift

Received: December 14, 2011
Revised: March 14, 2012
Published: March 22, 2012

only a negligible amount of acetone partitions into the aqueous phase. This would, however, only hold in an equilibrated system. Field measurements by van Pinxteren et al.[20] clearly showed that much higher concentrations of small carbonyl compounds could be found in cloudwater than predicted from their Henry coefficients.

The aim of the present study is the characterization of the OH-initiated oxidation of acetone in the aqueous phase. In particular, spectroscopic and kinetic properties of transient intermediates were investigated. Furthermore, qualitative and quantitative studies on the major oxidation products hydroxyacetone and methylglyoxal were done in order to develop a degradation mechanism in aqueous phase.

EXPERIMENTAL SECTION

Kinetic and spectroscopic investigations were conducted using a laser photolysis long path absorption (LP-LPA) setup (Figure 1).

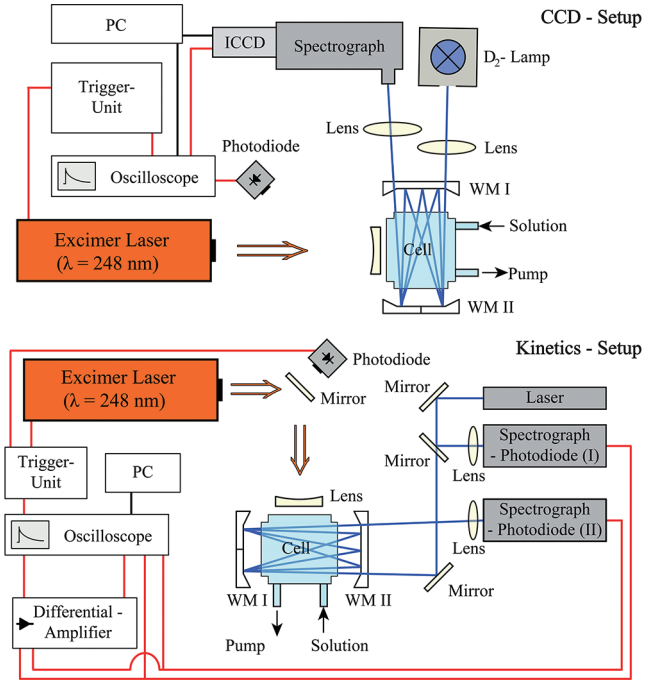

Figure 1. LP-LPA setup for spectroscopic (CCD - Setup) and kinetic (Kinetics - Setup) investigations.

Acetone (99.9%, Sigma Aldrich) was handled as received without further purification. Methylglyoxal was purified after the method from Staffelbach et al.[21] All other reactants (Sigma Aldrich or ABCR) were analytical grade or better. For the pH adjustment, perchloric acid or phosphate buffer were used. The concentration of hydrogen peroxide was verified with UV−visible (UV−vis) spectrometry. Solutions were prepared freshly with Milli-Q water (Millipore, MI).

CCD - Setup. The spectroscopic investigations of the peroxy radicals (RO_2) were done with a setup (Figure 1, CCD - Setup) including a gated ICCD camera (PI-MAX ICCD 1024 SB 25GenII, Princeton Instruments) coupled with a grating spectrograph in combination with a 200 W deuterium lamp. The analyzing light beam was passed through White cell optics adjusted for an absorption path length of 48 cm in the cell. The cell is made of suprasil with a volume of 28 mL. The photolysis of the radical precursor H_2O_2 was initiated by an excimer laser (LPX 201, Lambda Physics) with the active medium KrF. The measurements were performed in the temperature range of 283 to 328 K adjusted by a thermostat (F25, Julabo).

Kinetics - Setup. For the kinetic investigation of the recombination of the peroxy radicals, the setup was modified (Figure 1, Kinetics - Setup). A HeCd-laser (λ = 325 nm) served as the light source, and a differential amplifier system with two photodiodes (S1336-44BQ, Hamamatsu) was used as the detector. The differential amplifier system was used to improve the signal-to-noise ratio (SNR) of the detected signal. The combination of a monochromator and a photodiode was used to avoid interferences due to scattered light from the excimer laser. The signals were transferred to a digital storage oscilloscope (Data SYS 944, Gould), which was connected to a PC.

Competition Kinetics. The competition kinetics of the OH radicals was investigated by the thiocyanate system.[13,22,23] As the analytical light source, a diode laser (λ = 473 nm) (LasNova Series 40 blue BLK 7310T, LASOS) was used, and a photodiode (S1336-44BQ, Hamamatsu) served as the detector (Figure 1, Kinetic − Setup).

The thiocyanate competition kinetics was also used for the determination of the initial OH concentration needed for optical measurements. The initial OH concentration was calculated using the molar absorption coefficients of hydrogen peroxide and thiocyanate ($\varepsilon(SCN^-)$ = 60 ± 3 $M^{-1}cm^{-1}$, $\varepsilon(H_2O_2)$ = 25.65 ± 1 $M^{-1}cm^{-1}$), quantum yield of hydrogen peroxide (Φ = 1.02 ± 0.1)[23] for λ = 248 nm and the reference constant $k_{OH+SCN^-} = k_{ref} = 1.24 \times 10^{10}$ M^{-1} s^{-1} from Chin and Wine.[22]

Oxidation Experiments and Analytical Procedures. The OH initiated oxidation of acetone was examined with laser-induced photolysis of hydrogen peroxide. A KrF-laser (λ = 248 nm) with a mean energy of 250 mJ per pulse delivered into the measurement solution was used. A cuvette served as a reaction vessel where 0.1 mM of acetone was mixed with 1 mM of hydrogen peroxide. The solution was then irradiated with laser pulses varying between 1 and 150 pulses. For the detection of carbonyl compounds, an aliquot was derivatized with 2,4-dinitrophenylhydrazine. After storing the solution in the dark for 2 h, the sample was cleaned with solid phase extraction and analyzed with a high-performance liquid chromatography/mass spectrometry (HPLC-MS) system (Ultimate 3000, Dionex). The separation was performed with a reversed phase C_{18}-column (Waters SunFire 2.1 × 100 mm, 3.5 μm) and a binary eluent (H_2O:CH_3CN) with an addition of 0.2% acetic acid each. The analytes were detected with a single quadrupole mass spectrometer equipped with electrospray ionization, which was used in the negative mode. Capillary electrophoresis with ultraviolet detection (CE-UV; Spectra Phoresis 1000, Thermo Separation Products) was used to analyze the produced organic acids oxalic acid and acetic acid. The method used for acid analysis is explained in detail by Neusüss et al.[24]

RESULTS AND DISCUSSION

The photolysis of hydrogen peroxide at λ = 248 nm was applied to generate hydroxyl radicals (reaction R-9), which react with organic compounds via H-abstraction (reaction R-10). In an oxygen-saturated aqueous solution, the alkyl radical is directly converted into the corresponding peroxy radical (reaction R-11) with $k_3 = 3.0 \times 10^9$ M^{-1} s^{-1}.[25] A detailed mechanism is listed in Table 1.

dx.doi.org/10.1021/jp2120753 | J. Phys. Chem. A 2012, 116, 6317−6326

Table 1. Full Reaction Mechanism with Rate Constants Used to Simulate the Experiments

	Reactions	Parameter	Comment
	Equilibria	pK_a	
R-1	$H_2O \rightleftarrows H^+ + OH^-$	13.999	33
R-2	$H_2O \rightleftarrows O2^+ + H^+$	4.57	33
	Acid−Base Reactions		
R-3	$H^+ + OH^- \rightarrow H_2O$	1.4×10^{11} M^{-1} s^{-1}	33
R-4	$H_2O \rightarrow H^+ + OH^-$	$k_3 \times K_1/[H_2O]$	33
R-5	$H_2O \rightarrow O_2^- + H^+$	$k_6 \times K_2$	33
R-6	$O_2^- + H^+ \rightarrow HO_2$	5×10^{10} M^{-1} s^{-1}	33
R-7	$HO_2 + OH^- \rightarrow O_2^- + H_2O$	5×10^{10} M^{-1} s^{-1}	33
R-8	$O_2^- + H_2O \rightarrow HO_2 + OH^-$	$k_7 \times K_1/K_2 \times [H_2O]$	33
	Chemical Reactions		
R-9	$H_2O_2 + h\nu \rightarrow 2 \times OH$		
R-10	$CH_3C(O)CH_3 + OH \rightarrow CH_3C(O)CH_2$	1.3×10^9 M^{-1} s^{-1}	best fit,[13]
R-11	$CH_3C(O)CH_2 + O_2 \rightarrow CH_3C(O)CH_2O_2$	3.0×10^9 M^{-1} s^{-1}	25
R-12	$2 \times OH \rightarrow H_2O_2$	3.6×10^9 M^{-1} s^{-1}	52
R-13	$OH + H_2O_2 \rightarrow H_2O + HO_2$	3.0×10^7 M^{-1} s^{-1}	53
R-14	$OH + HO_2 \rightarrow H_2O + O_2$	6.0×10^9 M^{-1} s^{-1}	52
R-15	$OH + O_2^- \rightarrow OH^- + O_2$	1.1×10^{10} M^{-1} s^{-1}	54
R-16	$2 \times HO_2 \rightarrow H_2O_2 + O_2$	9.8×10^5 M^{-1} s^{-1}	55
R-17	$HO_2 + H_2O_2 \rightarrow OH + O_2 + H_2O$	5×10^{-1} M^{-1} s^{-1}	33
R-18	$2 \times O_2^- + 2 \times H_2O \rightarrow H_2O_2 + O_2 + 2 \times OH^-$	$1 \times 10^2/[H_2O]$	55
R-19	$HO_2 + O_2^- \rightarrow HO_2^- + O_2$	8.4×10^7 M^{-1} s^{-1}	55
R-20	$CH_3C(O)CH_2O_2 + CH_3C(O)CH_2O_2 \rightarrow P1$	7.1×10^8 M^{-1} s^{-1}	fitted
R-21	$CH_3C(O)CH_3 + h\nu \rightarrow CH_3 + CH_3C(O)$		25
R-22	$CH_3 + O_2 \rightarrow CH_3O_2$	3.0×10^9 M^{-1} s^{-1}	25
R-23	$CH_3C(O) + O_2 \rightarrow CH_3C(O)O_2$	3.0×10^9 M^{-1} s^{-1}	25
R-24	$2 \times CH_3O_2 \rightarrow P2$	1.1×10^8 M^{-1} s^{-1}	56
R-25	$2 \times CH_3C(O)O_2 \rightarrow P3$	3.2×10^8 M^{-1} s^{-1}	assumed[51,56]
R-26	$CH_3O_2 + CH_3C(O)O_2 \rightarrow P4$	3.2×10^8 M^{-1} s^{-1}	assumed[51,56]
R-27	$CH_3O_2 + CH_3C(O)CH_2O_2 \rightarrow P5$	3.2×10^8 M^{-1} s^{-1}	assumed[51,56]
R-28	$CH_3C(O)O_2 + CH_3C(O)CH_2O_2 \rightarrow P6$	3.2×10^8 M^{-1} s^{-1}	assumed[51,56]
R-29	$CH_3O_2 + O_2^- \rightarrow P7$	1.0×10^9 M^{-1} s^{-1}	assumed[25,51]
R-30	$CH_3O_2 + HO_2 \rightarrow P8$	1.0×10^8 M^{-1} s^{-1}	assumed[25,51]
R-31	$CH_3C(O)O_2 + O_2^- \rightarrow P9$	1.0×10^9 M^{-1} s^{-1}	assumed[25,51]
R-32	$CH_3C(O)O_2 + HO_2 \rightarrow P10$	1.0×10^8 M^{-1} s^{-1}	assumed[25,51]
R-33	$CH_3C(O)CH_2O_2 + O_2^- \rightarrow P11$	1.0×10^9 M^{-1} s^{-1}	assumed[25,51]
R-34	$CH_3C(O)CH_2O_2 + HO_2 \rightarrow P12$	1.0×10^8 M^{-1} s^{-1}	assumed[25,51]

$$H_2O_2 + h\nu \rightarrow 2OH \quad \text{(R-9)}$$

$$OH + RH \rightarrow R + H_2O \quad \text{(R-10)}$$

$$R + O_2 \rightarrow RO_2 \quad \text{(R-11)}$$

Acetonylperoxy Radical - Spectrum. The resulting spectrum of the acetonylperoxy radical measured in an O_2-saturated solution containing 2×10^{-4} M hydrogen peroxide and 6×10^{-4} M acetone is shown in Figure 2. The spectrum was measured 62 μs after the laser pulse, which is the time when reactions R-10 and R-11 were completed.

A correction of the spectrum was performed for the contribution of direct acetone photolysis. A spectrum of an O_2-saturated solution of 3.5×10^{-4} M acetone was measured. This acetone concentration corresponds to the contribution of light absorption by acetone in the solution with the OH precursor. The obtained spectrum was subtracted from the first spectrum. The resulting spectrum is shown in Figure 3 and was smoothed with the negative exponential function by means of the SigmaPlot 10 program. The absolute decadic extinction coefficient of the acetonylperoxy radical was calculated by using a modeled peroxy radical concentration, which was determined

dx.doi.org/10.1021/jp2120753 | J. Phys. Chem. A 2012, 116, 6317−6326

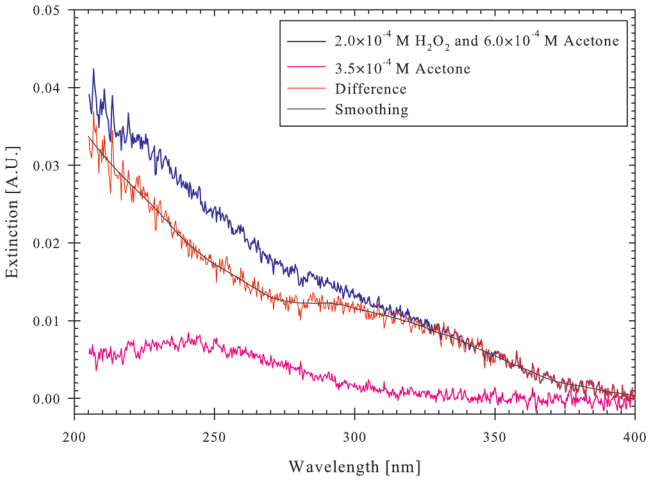

Figure 2. The correction of the spectrum due to the contribution of the acetone photolysis.

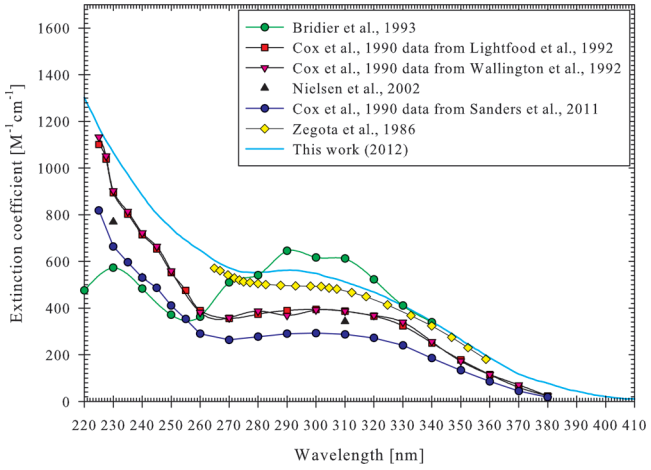

Figure 3. Spectrum of the acetonylperoxy radical compared with the literature.

as [Acetonylperoxy] = 6.18 × 10^{-7} M at t = 62 μs. Furthermore, the contribution of the absorption of the O_2^- radical was subtracted by using the modeled O_2^- radical concentration of $[O_2^-]$ = 3.95 × 10^{-8} M and using the O_2^- radical spectrum published by Behar et al.[26] with ε_{10}(325 nm) = 58 L M^{-1} s^{-1}.

The spectra in Figure 2 show two characteristic absorption features in the 220−400 nm region: a strong band at the wavelength <260 nm, and a fairly weak band centered at ∼300 nm. The measured spectrum is in good agreement with the absorption spectrum from Zegota et al.,[16] which was measured in the aqueous phase using pulse radiolysis. Differences can be found in comparison with the gas phase spectra measured by Cox et al.,[27] Nielsen et al.,[28] and Bridier et al.[29] The shapes of the spectra measured by Cox et al.[27] and Nielsen et al.[28] are similar to the spectrum measured here.

The value of gas phase extinction coefficient was revised several times by Lightfood et al.,[30] Wallington et al.[31] and Sander et al.[32] The spectrum by Bridier et al.[29] also shows inconsistencies in comparison with the spectra measured in the gas phase.

Kinetics of the Acetonylperoxy Recombination Reaction. The peroxy radical concentration has been calculated using a COPASI model. The main model mechanism is given in Table 1. This model takes into account the pH-dependent side reactions of HO_x radicals formed by the OH reaction with H_2O_2.[33] Furthermore, possible side reactions of peroxy radicals formed from direct acetone photolysis were included.

To test this model, a measurement of the formation of the peroxy radicals in an O_2-saturated solution containing 2 × 10^{-4} M hydrogen peroxide and 6 × 10^{-4} M acetone was performed. With the knowledge of the initial OH concentration, the best fit of this measurement was obtained with the rate constant k_2 = 1.3 × 10^8 M^{-1} s^{-1} (Figure 4). This value is comparable with the literature data.[12,34]

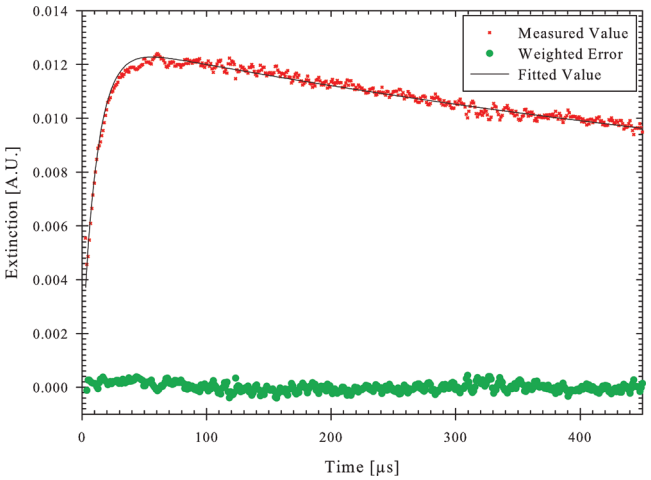

Figure 4. Copasi fit (---) for the absorbance change at λ = 325 nm due to reactions in an O_2 saturated solution containing 2 × 10^{-4} M hydrogen peroxide and 6 × 10^{-4} M acetone.

Calculations with a COPASI model showed that the concentration of the formed HO_2 radical is less than 4% of the maximum of the peroxy radical concentration. Hence, the turnover of the reaction of the acetonylperoxy radical with HO_2/O_2^- radical is small under the experimental conditions of the present study. Moreover, due to the equilibrium reaction R-2, i.e.,

$$HO_2 \rightleftarrows O_2^- + H^+ \qquad (pK_a = 4.57) \qquad \text{(R-2)}$$

and the adjusted pH = 6, the HO_2 radical is predominantly present in his deprotonated form, i.e., the superoxide radical O_2^-, and hence an even lower probability for a recombination of acetonylperoxy with HO_2 is expected compared to the corresponding process with O_2^-.

Due to a possible direct acetone photolysis, both the methylperoxy radical and the acetylperoxy radical can be formed by reactions R-21−R-23. The contribution of the cross reaction of the acetonylperoxy radical with these two radicals is small because the low quantum yield of the acetone photolysis is Φ = 0.061 at Φ = 270 nm[35] or Φ = 0.053 for the wavelength range 200−300 nm.[17,36] The obtained peroxy radical concentration from the photolysis of acetone is about 9.7 × 10^{-8} M for both acetylperoxy and methylperoxy radicals corresponding to about 16% of the initial acetonylperoxy radical concentration.

It should be considered that triplet state acetone may be formed following light absorption in the excimer laser photolyis. The triplet state acetone can undergo H-abstraction reactions with organic compounds and hydrogen peroxide in aqueous solution and produce alkyl radicals or hydroperoxy

dx.doi.org/10.1021/jp2120753 | J. Phys. Chem. A 2012, 116, 6317−6326

Table 2

(a) The Measured Rate Constants and Modeled Rate Constants for the Acetonylperoxy Radical Recombination Reaction in Aqueous Phase

T [K]	measurement k_{second} [M^{-1} s^{-1}]	model fit k_{second} [M^{-1} s^{-1}]
278	$(6.6 \pm 1.2) \times 10^8$	$(6.8 \pm 1.0) \times 10^8$
288	$(7.6 \pm 1.4) \times 10^8$	$(7.0 \pm 0.9) \times 10^8$
298	$(7.9 \pm 1.8) \times 10^8$	$(7.3 \pm 1.3) \times 10^8$
308	$(8.4 \pm 1.3) \times 10^8$	$(7.7 \pm 1.3) \times 10^8$
318	$(9.7 \pm 2.0) \times 10^8$	$(8.8 \pm 2.5) \times 10^8$

(b) The Measured Extinction Coefficient, Rate Constants and Activation Parameters for the Acetonylperoxy Radical Recombination Reaction in Aqueous Phase

reactant	$\varepsilon_{325\ nm}$ [M^{-1} cm^{-1}]	k_{second} [M^{-1} s^{-1}]	E_A [kJ mol^{-1}]	A [M^{-1} s^{-1}]	reference
acetone	415	4×10^8			16
	400	$(7.3 \pm 1.3) \times 10^8$	4.5 ± 3.3	$(4.7 \pm 2.7) \times 10^9$	this work

radicals.[37] Under the experimental conditions of the present study, however, the triplet state acetone is expected to be rapidly quenched by a diffusion-controlled reaction with dissolved molecular oxygen and produce singlet molecular oxygen.[38] At the concentration of dissolved oxygen in aqueous solution, $[O_2] = 5 \times 10^{-4}$ M, during the present study, oxygen suppresses the possible side reactions of the triplet state acetone as the quenching lifetime is calculated with $\tau = 0.2$ μs.

The resulting singlet state molecular oxygen will then again be quenched in aqueous solution by water molecules[39] and could, to a much smaller extent, also react with peroxy radicals with a rate constant near the diffusion limit[40] under spin inversion.

For the reaction between the triplet state acetone and hydrogen peroxide, an upper limit rate constant can be estimated as $k(H_2O_2) < 10^7$ M^{-1} s^{-1} based on a comparison of the H-bond dissociation energies and the rate constants of the reaction of triplet state acetone with organic compounds.[41] Under the present experimental conditions, the loss rate for triplet acetone by oxygen quenching relates to the loss rate by the reaction with H_2O_2 as 2400:1. In summary, the calculation with this estimated rate constant indicates that the influence of the triplet state acetone on the H-atom abstraction reaction with H_2O_2 is negligible under the used conditions.

In this study, the first temperature-dependent measurement of the acetonylperoxy radical recombination reaction in aqueous solution was performed by measuring the light intensity at the analyzing wavelength $\lambda = 325$ nm with ε_{10}(acetonylperoxy, 325 nm) = 440 M^{-1} cm^{-1}. The resulting intensity-vs-time profiles were evaluated by two different methods: First, a classical analysis for the determination of a second-order rate constant by plotting the reciprocal acetonylperoxy concentration over t was performed. Then, due to the above-mentioned possible interferences of HO_x and organic peroxyl radicals other than acetonylperoxy, a series of model runs was performed for all five temperatures with the mechanism depicted in Table 2. In these runs, the basic water and ion chemistry reactions (reactions R-1 and R-2 and reactions R-3−R-8) were kept T-independent. Where available, T-dependences from the literature were applied (reactions R-10, R-12−R-19, and R-24). Alkyl radical reactions with O_2 were set to k (298 K) = 3×10^9 M^{-1} s^{-1} and an activation energy of $E_A = 15$ kJ mol^{-1}.

The recombination kinetics of organic peroxyl radicals other than the acetonylperoxy radical (reactions R-24−R-28) were treated by the data available for the methylperoxy radical recombination in aqueous solution. The formation of organic hydroperoxides (reactions R-29−R-34) was treated by a T-independent estimate of the rate constants involving HO_2 of $k = 1 \times 10^8$ M^{-1} s^{-1} and those involving O_2^- of $k = 1 \times 10^9$ M^{-1} s^{-1}.

The calculations with the COPASI model showed that the recombination rate constant at $T = 298$ K was influenced by the side reaction with methylperoxy radical and the acetylperoxy radical. Taking into account the side reactions of peroxy radicals, a rate constant of $k = 7.3 \times 10^8$ M^{-1} s^{-1} was obtained (Figure 5).

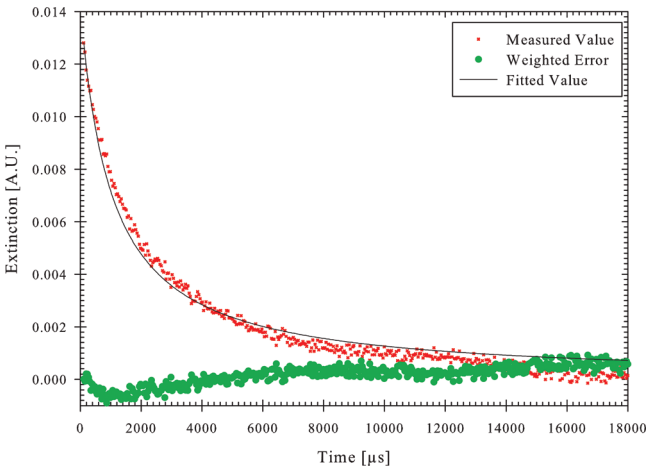

Figure 5. Copasi fit (---) for the decay of the acetonylperoxy radical at $T = 298$ K.

Without consideration of this side reactions, a value of $k = 7.9 \times 10^8$ M^{-1} s^{-1} was determined form the classical analysis at room temperature.

Because the influence of additional reactions besides the recombination was found to be non-negligible at room temperature, the simulation and fitting procedure was performed for all temperatures where measurements were performed.

The temperature dependencies obtained both analytically and by the model approach are both shown together in the Arrhenius plot of Figure 6. The obtained rate constants for both types of analysis are listed in Table 2a. Table 2b lists the used absorption coefficients and the resulting overall activation parameters resulting from the modeling analysis.

In Figure 7, the idea of the reaction mechanism after von Sonntag and Schuchmann[42] is shown. There are three possible ways of degradation of the tetroxide in aqueous phase, where two molecules of a carbonyl and hydrogen peroxide (Figure 7, A), one carbonyl compound, an alcohol and molecular oxygen (Figure 7, B), or two molecules of an alkoxy radical and

dx.doi.org/10.1021/jp2120753 | J. Phys. Chem. A 2012, 116, 6317−6326

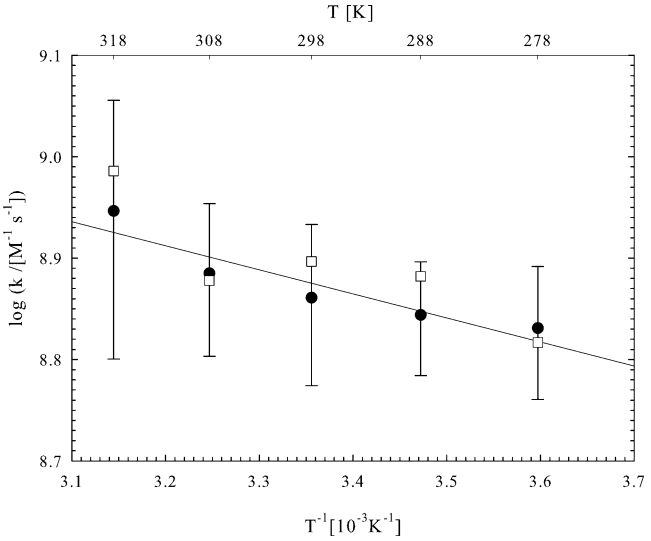

Figure 6. The Arrhenius plot for the recombination reaction of the acetonylperoxy radical: (●) modeling and fit resulting rate constants; (□) rate constant from classical kinetic second-order analysis. Each single experiment was simulated, and the error was calculated as the standard deviation from the set of the single fitting results.

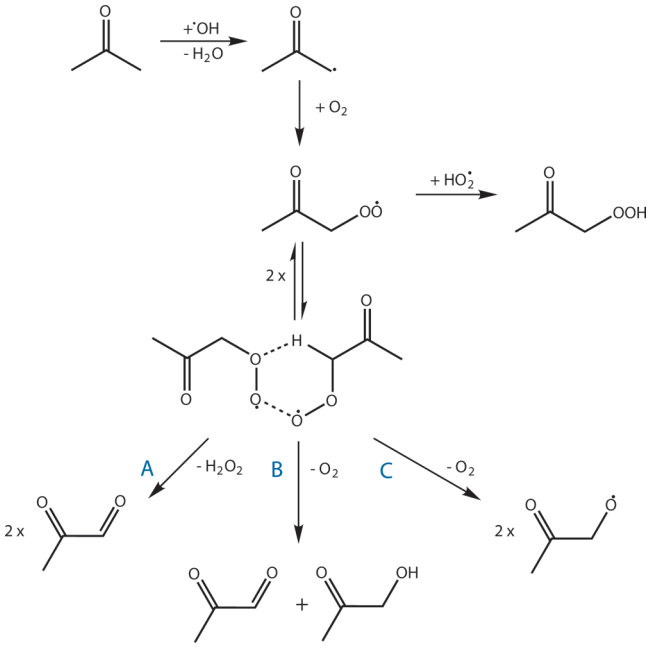

Figure 7. Reaction scheme for the OH-initiated oxidation of acetone in aqueous solution.

molecular oxygen (Figure 7, C) can be formed.[42] Different from the liquid phase, only the reaction ways B and C are possible in the gas phase,[43] due to the fact that the transition state of reaction A probably includes two water molecules.[42]

The analytical measurements described later will result in a branching ratio for the different depicted product formation channels.

Competition Kinetics. Kinetic investigations of the OH-initiated oxidation of methylglyoxal and pyruvic acid were done to determine the rate constants of these reactions. From the competing reaction of the OH radical with the thiocyanate anion SCN^-, the yield of the resulting $(SCN)_2^-$ anion radical can be used for calculating the rate constant of the OH reaction with the organic compound. In the previous study of Ervens et al.[13] from our laboratory, this method is described in detail.

In the case of an absorption at the photolysis wavelength by the reactant, the maximum absorption of the $(SCN)_2^-$ radical for the reaction without reactant has to be corrected by the inner filter effect of the reactant.

$$\frac{\left(E_{[(SCN)_2^-]_0}\right)_x}{E_{[(SCN)_2^-]_x}} = 1 + \frac{k_{OH+Reactant}[Reactant]}{k_{Reference}[SCN^-]}$$

$\left(E_{[(SCN_2^-)]_0}\right)_x$ is the maximum absorption of the $(SCN)_2^-$ radical with correction for the particular reactant concentration marked with the *x*. $E_{[(SCN_2^-)]_x}$ is the reduced absorption of the $(SCN)_2^-$ radical for the reaction with addition of a particular reactant concentration *x*.

In Figures 8 and 9, the Arrhenius plots for the reactions of OH with methylglyoxal and pyruvic acid are depicted. The rate

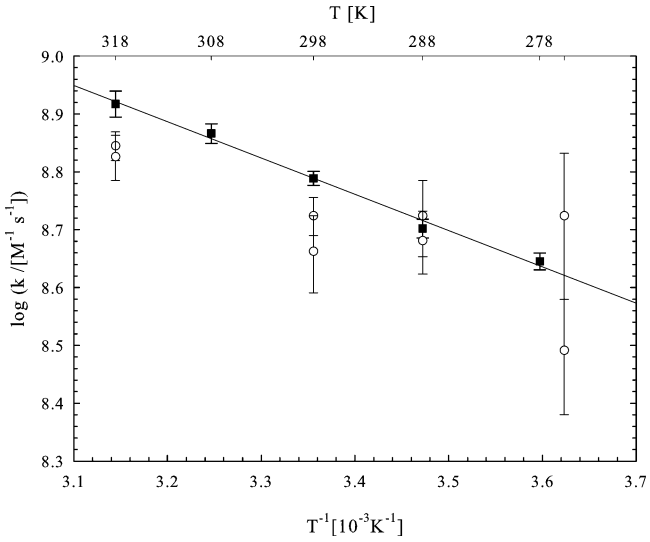

Figure 8. Arrhenius plot for the reactions of OH with methylglyoxal (■) (pH = nat) from this work and (○) (pH = 2) from Monod et al.[45]

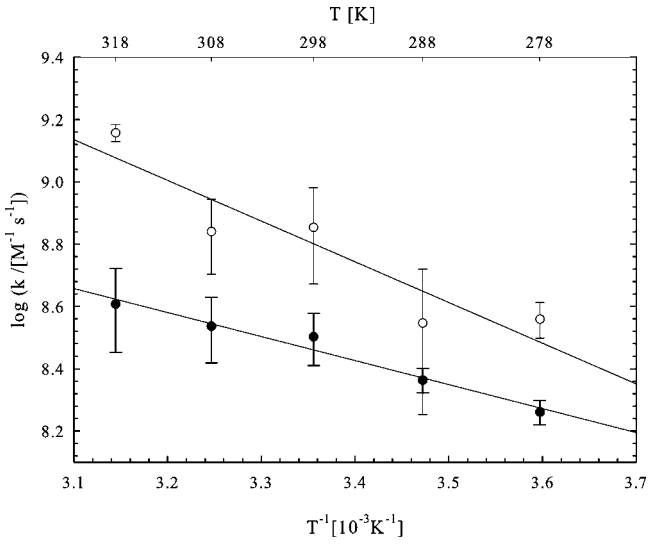

Figure 9. Arrhenius plot for the reactions of OH with (●) pyruvic acid (pH = 0) and (○) pyruvate (pH = 6) from this work.

dx.doi.org/10.1021/jp2120753 | J. Phys. Chem. A 2012, 116, 6317–6326

Table 3. The Measured Rate Constants and Activation Parameters for the OH Initiated Oxidation of Methylglyoxal and Pyruvic Acid in Aqueous Phase

reactant	pH	k_{second} [$M^{-1}s^{-1}$]	E_A [kJ mol^{-1}]	A [M^{-1} s^{-1}]	reference
methyl-glyoxal	6	$(1.1 \pm 0.1) \times 10^9$	13 ± 6	$(2.9 \pm 0.3) \times 10^{11}$	13
		$(5.3 \pm 0.4) \times 10^8$	9 ± 3	$(2.0 \pm 1.1) \times 10^{10}$	45
		$(6.1 \pm 0.2) \times 10^8$	12 ± 2	$(7.8 \pm 0.2) \times 10^9$	this work
pyruvic acid	0	$(1.2 \pm 0.4) \times 10^8$	23 ± 4	$(1.0 \pm 0.1) \times 10^{12}$	13
		$(3.2 \pm 0.6) \times 10^8$	15 ± 5	$(1.1 \pm 0.1) \times 10^{11}$	this work
	5.5	$(7.0 \pm 2.0) \times 10^8$	19 ± 4	$(1.3 \pm 0.1) \times 10^{12}$	13
	9	2.7×10^7			46
	6	$(7.1 \pm 1.8) \times 10^8$	25 ± 19	$(1.5 \pm 0.4) \times 10^{13}$	this work

constant for the pyruvic acid ($pK_a = 2.45$)[44] was determined at pH = 0 and pH = 6 for its protonated and deprotonated forms.

Table 3 also shows the calculated activation parameters of the reactions. Compared with the two available rate constants from the literature, the current one obtained for the reactions of OH and methylglyoxal in this work is in good agreement. The slightly larger constant of $k = 1.1 \times 10^9$ M^{-1} s^{-1} measured by Ervens et al.[13] could be attributed to a missing purification of the methylglyoxal. The inner filter effect is negligible under the used conditions. Furthermore, Monod et al.,[45] used the dark Fenton reaction at pH = 2 as an OH source.

Differences can be found by comparison of the obtained rate constants and Arrhenius expressions at different pH values from the OH-initiated oxidation of the pyruvic acid. The reason for this could be the contribution of the electron transfer from the unprotonated form of the acid. In this work, a liquid standard of the pyruvic acid was used instead of the sodium salt used by Ervens et al.[13] In the study of Ervens et al.[13] the rate constant was not corrected for the inner filter effect of the solution, therefore the rate constant for $T = 298$ K should be for pyruvate $k_{corr} = 3.8 \times 10^8$ M^{-1} s^{-1} and for pyruvic acid $k_{corr} = 6.8 \times 10^7$ M^{-1} s^{-1}. Nevertheless, the discrepancy observed at pH = 0 between the work of Ervens et al.[13] and the current study concerning the activation energy of the Arrhenius expression is not clear. The rate constant of $k = 2.7 \times 10^7$ M^{-1} s^{-1} measured by Kraljic[46] was obtained by using the *p*-nitrosodimethylaniline (PNDA) as the reference system instead of the thiocyanate system. The PNDA can act as reducing and oxidation agent. The oxidation of the pyruvic acid with the PNDA as a side reaction could explain the smaller rate constant.[47,48]

Oxidation Products and Mechanism. In Figures 10 and 11, the time profiles of acetone and the measured oxidation products are shown. The results of this study are similar to the concentration profiles obtained by lamp photolysis experiments of earlier studies.[18,19]

The acetone concentration (Figure 10) shows no clear decay for the first 10 laser pulses. Calculations with a small kinetic model have shown that, for the concentration of 1 mM hydrogen peroxide, only one-fifth of the formed OH radicals (~7 μM for the first laser pulse) react with acetone. The decay of 1 μM acetone per pulse is in the range of the error of measurement and is therefore not measurable for the first 10 laser pulses. Most OH radicals react with hydrogen peroxide or preferably with themselves, producing HO_2 radicals and hydrogen peroxide.

Pyruvic acid and acetic acid (Figure 10) were found to be the major intermediates in the oxidation of acetone but show a retarded increase of the concentration from the 20th laser pulse on. The primary products methylglyoxal and hydroxyacetone

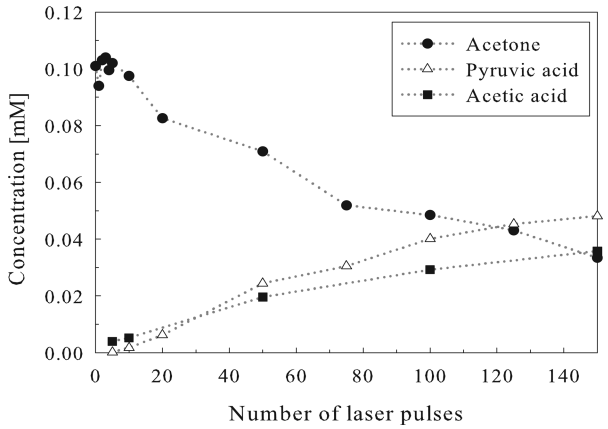

Figure 10. Concentration profiles of acetone and the main oxidation products pyruvic acid and acetic acid as a function of the number of laser pulses.

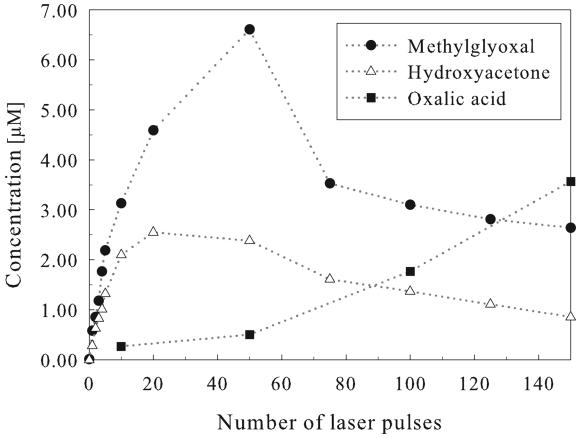

Figure 11. Concentration profiles of the oxidation products methylglyoxal, hydroxyacetone, and oxalic acid dependent on the number of laser pulses.

(Figure 11) were detected in concentrations smaller by one order of magnitude compared to pyruvic acid and acetic acid. Methylglyoxal and hydroxyacetone are "early" oxidation products with a strong increase of the concentrations within the first 5 laser pulses where methylglyoxal is produced twice as much as hydroxyacetone. Both of these products reach their maximum concentration after the 20th or 50th pulse. The concentration of the oxalic acid (Figure 11) shows a strong increase from the 50th laser pulse on, suggesting that oxalic acid is a "late" oxidation product as well as the major organic end product of the acetone oxidation.

dx.doi.org/10.1021/jp2120753 | J. Phys. Chem. A 2012, 116, 6317–6326

On the basis of the measured concentration profiles of acetone and its oxidation products, a reaction scheme (Figures 7 and 12) was compiled using available information.[16,18,42,49,50]

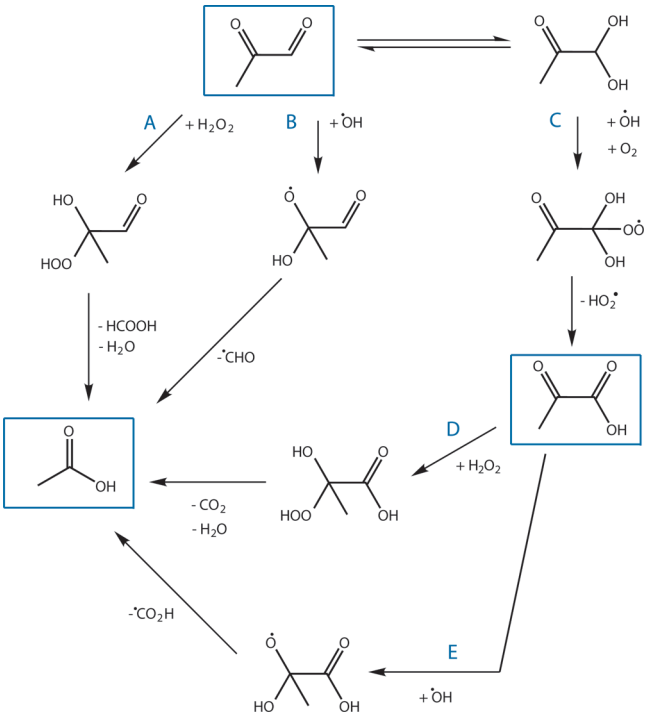

Figure 12. Degradation mechanism of methylglyoxal.

As proposed by Zegota et al.[16] and as discussed earlier in our present contribution, acetone reacts with OH radicals under H-abstraction. Due to the fast reaction with oxygen, acetonylperoxy radicals are formed immediately. These can react with themselves or with HO_2 radicals when available. In the latter reaction, acetonylhydroperoxide is formed, which is not considered in this study. The formation of the primary oxidation products methylglyoxal, hydroxyacetone, and acetic acid can be explained by the recombination of two acetonylperoxy radicals and the decomposition of the formed tetroxide. Two pathways can explain the production of methylglyoxal. Either the tetroxide degrades to form two molecules of methylglyoxal under elimination of hydrogen peroxide (Figure 7, A), or it forms methylglyoxal and hydroxyacetone whereby oxygen is released (Figure 7, B). A third way of degradation is the formation of two alkoxy radicals under the release of oxygen (Figure 7, C). The alkoxy radicals are expected to decompose, leading to the formation of an acetyl radical. This reacts immediately with oxygen to form the acetylperoxy radical.

With the estimated decay of 1 μM acetone and the measured concentrations of the primary products methylglyoxal and hydroxyacetone for the first laser pulse the ratio of the two described reaction pathways can be calculated yielding the result listed in Table 4.

Since on pathway B in Figure 7 hydroxyacetone and methylglyoxal is produced, the excess concentration of methylglyoxal is formed on the second way under elimination of hydrogen peroxide. For comparison, this ratio is also listed for the earlier studies.[16,18,19] The result of the present study is most consistent with the ratio found in the study by Stefan and Bolton.[18]

Table 4. Ratio of the Two Possible Reaction Pathways A and B for the Production of Methylglyoxal (Figure 7)

reaction A	reaction B	reference
40–45%	20%	Zegota et al.[16]
25%	60%	Stefan and Bolton[18]
60%	26%	Poulain et al.[19]
30%	56%	this work

A significant increase of the concentration of acetic acid was measured together with the strong increase of the pyruvic acid concentration after 50 laser pulses. Pyruvic acid is a known oxidation product of methylglyoxal. The formation was discussed before by Stefan and Bolton[18] and can be explained with the elimination of an HO_2 radical after H-abstraction of the aldehydic H-atom of methylglyoxal (Figure 12, C). As shown in Figure 12, two possible reaction mechanisms might explain the production of acetic acid.

First, the attack of an OH radical on the keto function of methylglyoxal might occur, which would lead to the formation of an alkoxy radical (Figure 12, B). The reaction was described by Zegota et al.[16] as a possible, but not favored reaction of acetone. In the decomposition, acetic acid and a formyl radical would be formed. However, a dark reaction of methylglyoxal with hydrogen peroxide is also a possible reaction (Figure 12, A). The formation of acetic acid and formic acid in this reaction was first described by Friedemann.[49] Stefan and Bolton[18] studied the dark reaction of the pyruvic acid with hydrogen peroxide and obtained a reaction rate of $k = 0.11\ M^{-1}\ s^{-1}$. The reaction was mechanistically explained by an attack of the hydrogen peroxide on the double bond of the keto group with a subsequent decarboxylation (Figure 12, D). These authors also proposed OH-initiated mechanisms such as the formation of a ketene and the H-abstraction from the hydrated pyruvic acid and generation of an alkoxy radical. Since the H-abstraction from a hydroxyl group is energetically not favored,[50] the alkoxy radical could also be formed due to the mentioned attack of the OH radical on the keto function. A decomposition can lead to the formation of acetic acid (Figure 12, E).

CONCLUSION

A spectroscopic investigation of the UV-spectrum of the acetonylperoxy radical was performed. Then, the temperature-dependent recombination reaction of the transient acetonylperoxy radical in the aqueous phase was studied. In kinetic investigations, the rate constant of the OH radical reactions with methylglyoxal, pyruvate, and pyruvic acid were determined. Furthermore, the identification and quantification of the OH-driven oxidation products of acetone dependent on the number of the laser pulses was performed. The main reaction pathways were quantified, and the result was found to be consistent with the results of Stefan and Bolton.[18] Apart from the pyruvic acid, acetic acid was found in high concentrations, which was explained by the known dark reaction as well as a conceivable attack of the OH radical on the keto-function of methylglyoxal and pyruvic acid.

The suggested mechanistic scheme should be used in atmospheric aqueous phase mechanisms, and formerly applied rate constant should be revised where necessary.

dx.doi.org/10.1021/jp2120753 | J. Phys. Chem. A 2012, 116, 6317–6326

AUTHOR INFORMATION

Corresponding Author

*Tel: +49-341-235-2446. Fax: +49-341-235-2325. E-mail: herrmann@tropos.de.

Present Address

‡Deutsches BiomasseForschungsZentrum, Ber. Thermo-chemische Konversion, Torgauer Str. 116, D-04347 Leipzig, Germany.

Notes

The authors declare no competing financial interest.

ACKNOWLEDGMENTS

The authors, and especially H.H., would like to dedicate this contribution to our friend A.R. Ravishankara with whom we had a lot of very fruitful exchanges over the years with emphasis on 'multiphase chemistry'. The project ACETOX was financially supported by the German Research Foundation DFG under HE3086/8-1 and HE3086/8-2.

REFERENCES

(1) Hallquist, M.; Wenger, J. C.; Baltensperger, U.; Rudich, Y.; Simpson, D.; Claeys, M.; Dommen, J.; Donahue, N. M.; George, C.; Goldstein, A. H.; et al. *Atmos. Chem. Phys.* **2009**, *9*, 5155−5236.

(2) Kanakidou, M.; Seinfeld, J. H.; Pandis, S. N.; Barnes, I.; Dentener, F. J.; Facchini, M. C.; Van Dingenen, R.; Ervens, B.; Nenes, A.; Nielsen, C. J.; et al. *Atmos. Chem. Phys.* **2005**, *5*, 1053−1123.

(3) Jacob, D. J.; Field, B. D.; Jin, E. M.; Bey, I.; Li, Q. B.; Logan, J. A.; Yantosca, R. M.; Singh, H. B. *J. Geophys. Res.-Atmos.* **2002**, DOI: 10.1029/2001JD000694.

(4) Singh, H.; Chen, Y.; Tabazadeh, A.; Fukui, Y.; Bey, I.; Yantosca, R.; Jacob, D.; Arnold, F.; Wohlfrom, K.; Atlas, E.; et al. *J. Geophys. Res.-Atmos.* **2000**, *105*, 3795−3805.

(5) Singh, H. B.; Ohara, D.; Herlth, D.; Sachse, W.; Blake, D. R.; Bradshaw, J. D.; Kanakidou, M.; Crutzen, P. J. *J. Geophys. Res.-Atmos.* **1994**, *99*, 1805−1819.

(6) Singh, H. B.; Salas, L. J.; Chatfield, R. B.; Czech, E.; Fried, A.; Walega, J.; Evans, M. J.; Field, B. D.; Jacob, D. J.; Blake, D.; et al. *J. Geophys. Res.-Atmos.* **2004**, *109*, D15S07−D15S20.

(7) Gierczak, T.; Burkholder, J. B.; Bauerle, S.; Ravishankara, A. R. *Chem. Phys.* **1998**, *231*, 229−244.

(8) Kanakidou, M.; Singh, H. B.; Valentin, K. M.; Crutzen, P. J. *J. Geophys. Res.-Atmos.* **1991**, *96*, 15395−15413.

(9) Jaegle, L.; Jacob, D. J.; Wennberg, P. O.; Spivakovsky, C. M.; Hanisco, T. F.; Lanzendorf, E. J.; Hintsa, E. J.; Fahey, D. W.; Keim, E. R.; Proffitt, M. H.; et al. *Geophys. Res. Lett.* **1997**, *24*, 3181−3184.

(10) Muller, J. F.; Brasseur, G. *J. Geophys. Res.-Atmos.* **1999**, *104*, 1705−1715.

(11) Singh, H. B.; Hanst, P. L. *Geophys. Res. Lett.* **1981**, *8*, 941−944.

(12) Buxton, G. V.; Greenstock, C. L.; Helman, W. P.; Ross, A. B. *J. Phys. Chem. Ref. Data* **1988**, *17*, 513−886.

(13) Ervens, B.; Gligorovski, S.; Herrmann, H. *Phys. Chem. Chem. Phys.* **2003**, *5*, 1811−1824.

(14) Herrmann, H. *Chem. Rev.* **2003**, *103*, 4691−4716.

(15) Gligorovski, S.; Herrmann, H. *Phys. Chem. Chem. Phys.* **2004**, *6*, 4118−4126.

(16) Zegota, H.; Schuchmann, M. N.; Schulz, D.; Vonsonntag, C. *Z. Naturforsch. B* **1986**, *41*, 1015−1022.

(17) Stefan, M. I.; Hoy, A. R.; Bolton, J. R. *Environ. Sci. Technol.* **1996**, *30*, 2382−2390.

(18) Stefan, M. I.; Bolton, J. R. *Environ. Sci. Technol.* **1999**, *33*, 870−873.

(19) Poulain, L.; et al. *Chemosphere* **2010**, *81*, 312−320.

(20) van Pinxteren, D.; Plewka, A.; Hofmann, D.; Muller, K.; Kramberger, H.; Svrcina, B.; Bachmann, K.; Jaeschke, W.; Mertes, S.; Collett, J. L.; et al. *Atmos. Environ.* **2005**, *39*, 4305−4320.

(21) Staffelbach, T. A.; Orlando, J. J.; Tyndall, G. S.; Calvert, J. G. *J. Geophys. Res.* **1995**, *100*, 14189−14198.

(22) Chin, M.; Wine, P. H. *J. Photochem. Photobiol. A* **1992**, *69*, 17−25.

(23) Herrmann, H.; Hoffmann, D.; Schaefer, T.; Braeuer, P.; Tilgner, A. *Chem. Phys.Chem.* **2010**, *11*, 3796−3822.

(24) Neusüss, C.; Pelzing, M.; Plewka, A.; Herrmann, H. *J. Geophys. Res.-Atmos.* **2000**, *105*, 4513−4527.

(25) Neta, P.; Huie, R. E.; Ross, A. B. *J. Phys. Chem. Ref. Data* **1990**, *19*, 413−513.

(26) Behar, D.; Czapski, G.; Rabani, J.; Dorfman, L. M.; Schwarz, H. A. *J. Phys. Chem.* **1970**, *74*, 3209−3213.

(27) Cox, R. A.; Munk, J.; Nielsen, O. J.; Pagsberg, P.; Ratajczak, E. *Chem. Phys. Lett.* **1990**, *173*, 206−210.

(28) Nielsen, O. J.; Johnson, M. S.; Wallington, T. J.; Christensen, L. K.; Platz, J. *Int. J. Chem. Kinet.* **2002**, *34*, 283−291.

(29) Bridier, I.; Veyret, B.; Lesclaux, R.; Jenkin, M. E. *J. Chem. Soc., Faraday Trans.* **1993**, *89*, 2993−2997.

(30) Lightfoot, P. D.; Cox, R. A.; Crowley, J. N.; Destriau, M.; Hayman, G. D.; Jenkin, M. E.; Moortgat, G. K.; Zabel, F. *Atmos. Environ.* **1992**, *26A*, 1805−1961.

(31) Wallington, T. J.; Dagaut, P.; Kurylo, M. J. *Chem. Rev.* **1992**, *92*, 667−710.

(32) Sander, S. P.; Abbatt, J.; Barker, J. R.; Burkholder, J. B.; Friedl, R. R.; Golden, D. M.; Huie, R. E.; Kolb, C. E.; Kurylo, M. J.; Moortgat, G. K. et al. *Chemical Kinetics and Photochemical Data for Use in Atmospheric Studies, Evaluation No. 17*; Jet Propulsion Laboratory: Pasadena, CA, 2011.

(33) Pastina, B.; A.LaVerne, J. *J. Phys. Chem. A* **2001**, *105*, 9316−9322.

(34) Gligorovski, S.; Rousse, D.; George, C. H.; Herrmann, H. *Int. J. Chem. Kinet.* **2009**, *41*, 309−326.

(35) Anpo, M.; Kubokawa, Y. *B. Chem. Soc. Jpn.* **1977**, *50*, 1913−1916.

(36) Hurley, S. M.; Dermota, T. E.; Hydutsky, D. P.; Castleman, A. W., Jr. *Int. J. Mass. Spectrom.* **2003**, *228*, 677−686.

(37) Nakashima, M.; Hayon, E. *J. Phys. Chem.* **1971**, *75*, 1910−1914.

(38) Wilson, T.; Schaap, A. P. *J. Am. Chem. Soc.* **1971**, *93*, 4126−4136.

(39) Wilkinson, F.; Ross, A. B.; Helman, W. P. *J. Phys. Chem. Ref. Data* **1995**, *24*, 663−1021.

(40) Darmanyan, A. P.; Foote, C. S.; Jardon, P. *J. Phys. Chem.* **1995**, *99*, 11854−11859.

(41) Porter, G.; Dogra, S. K.; Loufty, R. O.; Sugamori, S. E.; Yip, R. W. *J. Chem. Soc., Faraday Trans. I* **1973**, *69*, 1462−1474.

(42) von Sonntag, C.; Schuchmann, H. P. *Angew. Chem., Int. Ed.* **1991**, *30*, 1229−1253.

(43) Jenkin, M. E.; Hurley, M. D.; Wallington, T. J. *Phys. Chem. Chem. Phys.* **2008**, *10*, 4274−4280.

(44) Lide, D. R. *Handbook of Chemistry and Physics*, 76 ed.; CRC Press: New York, 1995.

(45) Monod, A.; Poulain, L.; Grubert, S.; Voisin, D.; Wortham, H. *Atmos. Environ.* **2005**, *39*, 7667−7688.

(46) Kraljic, I. *Chemistry of Ionisation and Excitation*; Taylor and Francis: London, 1967.

(47) Tanasescu, I.; Ruse, M. *Chem. Ber.* **1959**, *92*, 1265−1269.

(48) Tanasescu, I.; Ruse, M. *Chem. Ber.* **1962**, *96*, 1762−1764.

(49) Friedemann, T. E. *J. Biol. Chem.* **1927**, *73*, 331−334.

(50) Asmus, K.-D.; Möckel, H.; Henglein, A. *J. Phys. Chem.* **1973**, *77*, 1218−1221.

(51) Alfassi, Z. B. *The Chemistry of Free Radicals: Peroxyl Radicals*; John Wiley & Sons: Chichester, 1997.

(52) Elliot, A. J.; Buxton, G. V. *J. Chem. Soc., Faraday Trans.* **1992**, *88*, 2465−2470.

(53) Christensen, H.; Sehested, K.; Corfitzen, H. *J. Phys. Chem.* **1982**, *86*, 1588−1590.

(54) Christensen, H.; Sehested, K.; Bjergbakke, E. *Water Chem. Nucl. React. Syst.* **1989**, *5*, 141−144.

(55) Christensen, H.; Sehested, K. *J. Phys. Chem.* **1988**, *92*, 3007–3011.
(56) Herrmann, H.; Zellner, R. *Final Report: Removal and Interconversions of Oxidants in the Atmospheric Aqueous Phase*; University of Essen: Essen, Germany, 1996.